Journal of Materials Chemistry C

Accepted Manuscript

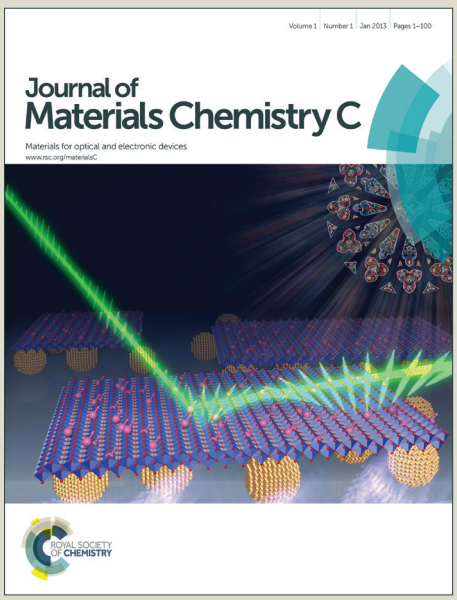

ROYAL SOCIETY OF CHEMISTRY

www.rsc.org/materialsC

Cite this: DOI: 10.1039/c0xx00000x

www.rsc.org/xxxxxx

ARTICLE TYPE

Highly Conductive and Uniform Graphene Oxide Modified PEDOT:PSS Electrode for ITO-Free Organic Light Emitting Diodes

Xinkai Wu[a], Jun Liu[a], Dongqing Wu[b], Yanru Zhao[b], Xindong Shi[a], Jing Wang[a], Saijun Huang[a] and Gufeng He[a]*

Received (in XXX, XXX) Xth XXXXXXXXX 20XX, Accepted Xth XXXXXXXXX 20XX
DOI: 10.1039/b000000x

We have successfully obtained highly transparent and conductive film by doping poly (3,4-ethylenedioxythiophene):poly(styrene sulfonate) (PEDOT:PSS) with graphene oxide (GO) and sodium dodecyl benzene sulfonate (SDBS). PEDOT:PSS hybrid film mixed with 0.02% GO:SDBS by weight exhibits a sheet resistance of 85 ohm per square and transmittance of 87% at 550 nm. The improvement of conductivity is mainly attributed to the weakening of coulombic attraction between PEDOT and PSS by the functional groups on GO nanosheets, and forming extended conductive network by connecting PEDOT chains with GO nanosheets. Using the optimized PEDOT:PSS hybrid film as anode, indium tin oxide (ITO)-free organic light emitting diodes (OLEDs) have been demonstrated on glass and polyethylene naphthalate (PEN) substrates, showing better performance than that with ITO as anode. This proves that such PEDOT:PSS and GO:SDBS hybrid film is a promising alternative to ITO for low cost flexible OLEDs.

1. Introduction

Recently the flexible organic light emitting diodes (OLEDs) have attracted tremendous attention owing to their lightness, thinness and the high mechanical flexibility.[1] The electrodes for flexible OLEDs should possess special characteristics, such as bendable, low-cost, highly conductive and transparent. Indium tin oxide (ITO) has been widely used as transparent electrode for organic optoelectronic devices. However, a few drawbacks of ITO including high price due to indium scarcity, complicated processing requirements, sensitive to acid and basic environments, prone to crack upon bending, render it unsuitable for application that requires stretchability or flexibility.[2] Over the past decade, several emerging materials including carbon nanotubes (CNTs),[3,4] graphene,[5,6] metallic nanowires,[7] and conducting polymers,[8,9] have been found as potential replacement for ITO. However, high roughness and instability limit the industrial applications of carbon nanotubes and metallic nanowires.

Graphene, a single layer of two-dimensional carbon lattice, is recognized to be a good electrode candidate for flexible OLEDs, due to its unique electrical, optical and mechanical properties.[10] Nevertheless, achieving low sheet resistance of graphene film requires a complicated process. Most of them are grown on metal foil by chemical vapor deposition (CVD) and the metal needs to be etched before transferring to other flexible substrates.[11] On the other hand, poly (3,4-ethylene dioxythiophene) (PEDOT) has been used as one of the most successful conducting polymer materials in optoelectronic applications due to its fairly high conductivity, transparency and good machinability. PEDOT doped with poly (styrenesulfonic acid) (PSS) can disperse in the aqueous solution and form counterion solution, which makes it more practicable. The conductivity of the PEDOT:PSS film highly depends on the ratio of PEDOT to PSS and particle size of the PEDOT:PSS dispersions in water.[12] But with regard to pristine PEDOT:PSS film, it is definitely too low (< 1 S cm^{-1}) as an electrode. Fortunately, the conductivity of PEDOT:PSS can be increased up to 2 or 3 orders of magnitude by adding some components, such as high boiling organic compound,[13] zwitterionic surfactant,[14] and metal electrolytes solution.[15] It is proved that these additives can result in larger PEDOT grains or increase phase separation between the conductive PEDOT and the insulating PSS. More PEDOT conductive pathways can form, but the roughness of film becomes higher.[16,17]

In particular, composites of graphene and PEDOT:PSS have attracted much researchers' attention due to the potential creation of synergistic effects on their electrical and thermal properties.[18] Chang et al.[19] use a surfactant sodium dodecyl benzene sulfonate (SDBS) to improve the dispersion of graphene in PEDOT:PSS solution, and the sheet resistance of SDBS:graphene and PEDOT:PSS hybrid films reaches 80 Ω sq^{-1} with 79% transmittance at 550 nm. However, the composite film has very high roughness which can be observed from AFM images. Moreover, the luminance (33 cd m^{-2}) and current density (0.85 mA cm^{-2}) of the OLEDs at 10 V are both smaller than those of the device with ITO anode (40 cd m^{-2} and 2.4 mA cm^{-2} respectively). Jo and his coworkers[20] have successfully demonstrated a simple and facile approach of preparing a stable aqueous dispersion system of reduced graphene oxide (rGO) nanosheets functionalized with PEDOT:PSS. The reduction

process is conducted by adding hydrazine into graphene oxide (GO) and PEDOT:PSS mixture, and later a hybrid film with a sheet resistance of 2300 Ω sq^{-1} at a 80% transmittance (at 550 nm) is obtained. The high sheet resistance of composite film limits its application as the electrode in OLEDs. Seol et al.[21] report that rGO nanosheets functionalized by a surfactant (phenyl isocyanate) could produce highly conductive film when mixing with PEDOT:PSS. Though the film obtains a sheet resistance of 68 Ω sq^{-1} at the optical transmittance of 86%, the reduction process of GO nanosheets causes severe aggregation in solution due to π-π interaction between rGO nanosheets, which makes terrible dispersion of rGO nanosheets in the solution of PEDOT:PSS. The complicated process and instability of the functionalized rGO and PEDOT:PSS mixture solution is not suitable to produce flexible conductive films in large scale. Therefore, to achieve high conductivity and transparency, low cost and roughness film in a simple method is still a challenge.

In this paper, we have produced smooth, highly conductive and transparent films by simply mixing water soluble GO with PEDOT:PSS solution. In order to improve the dispersion of GO in PEDOT:PSS solution, a surfactant SDBS was added, which could intercalate into layered GO and prevent their aggregation. As a result, the hybrid film achieved a sheet resistance of 85 ohm per square with the optical transmittance of 87% at 550 nm, and the film roughness is even lower than primitive PEDOT:PSS films. OLEDs fabricated with such anode could obtain the current density of 100 mA cm^{-2} only at 5.4 V, and reach 1000 cd m^{-2} luminance value at 4.6 V. The power efficiency of OLEDs using PEDOT:PSS anode with 0.02 wt% GO:SDBS is three times as high as the device with ITO anode. Our results demonstrate that PEDOT:PSS mixing with GO:SDBS can be used as an alternative anode to ITO for OLEDs.[22]

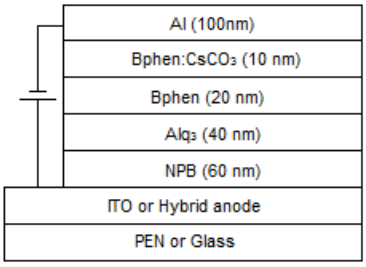

Fig. 1 Schematic cross-section of OLED device.

2. Experimental

2.1 Fabrication of PEDOT:PSS and GO:SDBS composite films

Graphite flakes and SDBS were purchased from Sigma Aldrich. All the chemicals were of analytical reagent grade, and used without further purification. PEDOT:PSS aqueous solution (Clevios PH 1000) was purchased from H. C. Starck. The concentration of PEDOT:PSS was 1.3% by weight, and the weight ratio of PSS to PEDOT was 2.5 in solution. Graphite powder was oxidized by the Hummers method to form graphene oxide.[23-25] The concentration of GO solution was kept about 3 mg ml^{-1}. SDBS (at a weight ratio of 8:1 to GO) was added into GO solution followed by an ultrasonication process for 1 h, and later the solution was stirred for 24 h in ambient atmosphere. Then the mixed solution was centrifuged at 10000 rpm, and the upper solution with redundant SDBS that did not intercalate into GO was removed, followed by adding the same volume of water to keep the concentration of GO. The above procedures were repeated several times to fully take off redundant SDBS from solution. The PEDOT:PSS was filtered through a syringe filter (0.45 μm pore size), then various amounts of GO:SDBS (0 wt%-0.1 wt%) and 6 wt% dimethyl sulfoxide (DMSO) were added into the PEDOT:PSS solution and stirred for 2 h. A homogenous film was obtained by spin coating the composite solution on clean polyethylene naphthalate (PEN) or glass substrate, and then was annealed on a hot plate at 150 °C for 15 min in ambient atmasphere. For multilayer films, the process was repeated for multiple times.

2.2 OLED devices

The glass or PEN substrates coated with PEDOT:PSS and GO:SDBS hybrid anodes were transferred into a high-vacuum system at a base pressure of 10^{-6} Torr for the following organic and metal layers deposition to finish the OLED fabrication. 60 nm N,N'-bis (naphthalen-1-yl)-N,N'-bis (phenyl)-benzidine (NPB) as the hole transporting layer, 40 nm tris-8-hydroxyquinoline aluminum (Alq_3) as emitting layer, 20 nm 4,7-diphenyl-1,10-phenanthroline (Bphen) as electron transporting and hole blocking layer, 10 nm 10% Cs_2CO_3 doped Bphen as electron injection layer and 100 nm aluminum (Al) as cathode were deposited successively. The active area defined by the overlap of the anode and the Al cathode was around 3 mm × 3 mm. The deposition rate was monitored in-situ by a quartz-crystal monitor. Fig. 1 shows the schematic cross-section of the fabricated device stack.

2.3. Film and device characterizations

The thickness of obtained PEDOT:PSS hybrid films were measured by D-120 profile-system (KLA-Tencor). UV-vis optical transmittance analysis of PEDOT:PSS with different ratios of GO:SDBS layers was carried out by MAPADA UV-3100PC spectrophotometer. The roughness and surface morphology of hybrid films were analyzed by a Digital Instruments Multimode Nanoscope atomic force microscope (AFM) with the tapping mode. The conductivity of the film was evaluated from sheet-resistance measurements by means of a four-point probe system. OLED device performances were characterized by computer controlled Keithley 2400 Source Meter and Topcon BM-7A Luminance Colorimeter.

3. Results and discussion

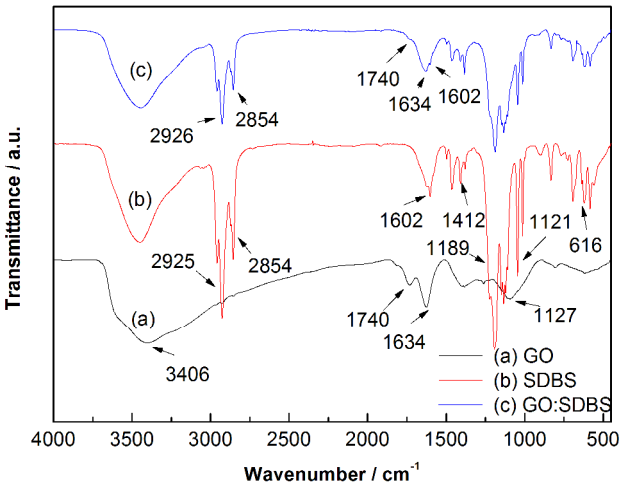

Fig. 2 FTIR spectra of GO (a), SDBS (b) and GO:SDBS (c).

Fig. 2 illustrates the Fourier-transform infrared spectroscopy (FTIR) spectra of GO, SDBS and GO:SDBS respectively. Two narrow peaks shown on spectrum (a) at 1740 cm^{-1} and 1634 cm^{-1} are from the carbonyl group (C=O stretching) of carboxylic acid. The broad absorption peaks at 3406 cm^{-1} and 1127 cm^{-1} are assigned to -OH groups and C-O-C bonds. These are all attributed to GO groups. For the SDBS (Fig. 2 (b)), the strong peaks at 2925 cm^{-1} and 2854 cm^{-1} are induced by C-H vibrations, and two small peaks at 1412 cm^{-1} and 1602 cm^{-1} are attributed to the vibration of the phenyl groups. Furthermore, the strong peaks at 1189 cm^{-1}, 1121 cm^{-1} and 616 cm^{-1} due to vibration of the S=O groups can be clearly seen from SDBS spectrum. On the other hand, GO:SDBS spectrum shows peaks at 2925 cm^{-1} and 2854 cm^{-1} due to C-H vibration peaks from SDBS, and 1740 cm^{-1} and 1634 cm^{-1} for the carbonyl group from GO, indicating that SDBS has intercalated into layered GO.

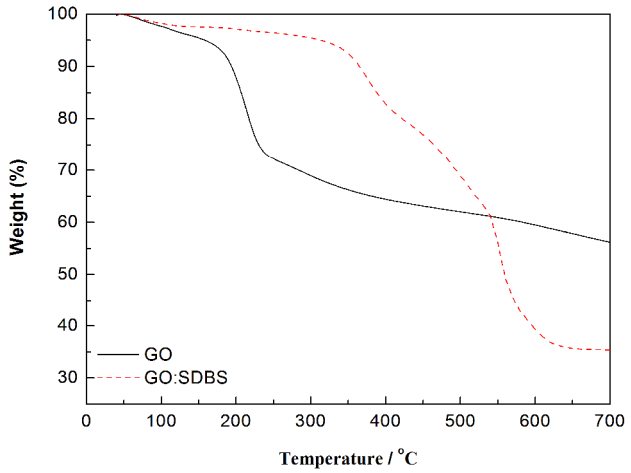

Fig. 3 Thermogravimetric analysis of GO and GO:SDBS.

To confirm that SDBS has intercalated into layered GO, the thermal stability of GO and GO:SDBS was investigated using Thermogravimetric analysis (TGA) by heating samples under a nitrogen atmosphere to 700 °C at a rate of 10 °C min^{-1}. As shown in Fig. 3, the main mass loss for GO is around 200 °C, and the overall weight loss was about 46%. This is ascribed to the decomposition of labile oxygen functional groups.[26] In contrast, the weight fraction loss of the GO:SDBS is measured to be about 68% at 350-700 °C. It may result from the decomposition of SDBS and labile oxygen functional groups on GO nanosheets. The improvement in thermal decomposition temperature indicates strong combination of SDBS and layered GO by relatively weaker π-π and hydrophobic interactions.[21]

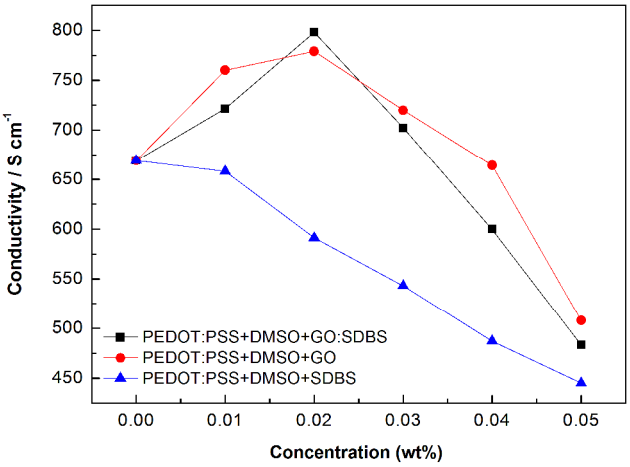

Fig. 4 The conductivity change tendency of PEDOT:PSS with 6 wt% DMSO mixing 0%-0.05 wt% GO:SDBS, SDBS and GO separately.

By adding GO:SDBS into PEDOT:PSS, the conductivity of formed hybrid film is remarkably increased from 0.1 S cm^{-1} to 115 S cm^{-1} until a concentration of 0.06 wt% (not shown). This improvement may be caused by the separation of PSS and PEDOT chains, because some functional groups on GO nanosheets (such as -COOH, -OH) and anionic surfactant SDBS may weaken the coulombic attraction between PEDOT and PSS.[27] These PEDOT chains can bond with GO nanosheets to extend the conductive network. However, a conductivity of 115 S cm^{-1} is not high enough as an electrode in OLEDs. In order to further enhance the conductivity of hybrid film, 6 wt% DMSO was added into the PEDOT:PSS and GO:SDBS mixed solution. As shown in Fig. 4, the conductivity of PEDOT:PSS hybrid film increases dramatically, and the highest value around 800 S cm^{-1} is obtained with 0.02 wt% GO:SDBS. However, the conductivity drops when the amount of GO:SDBS is further increased. It may be related to the reduction of oriented conductive network of PEDOT chains with higher GO concentration. In order to study this effect, SDBS and GO were separately mixed into PEDOT:PSS solution with DMSO. It can be found that the conductivity of hybrid film drops with increasing concentration of SDBS. This indicates that insulated SDBS may interfere with the conductive PEDOT pathways and lower down the conductivity of PEDOT:PSS hybrid films, and the role of SDBS here just improves the dispersion of GO in PEDOT:PSS solution. In contrast, the conductivity of PEDOT:PSS hybrid film reaches the maximum with 0.02 wt% GO. The variation trend is similar to PEDOT:PSS with GO:SDBS hybrid film, indicating that the conductivity of PEDOT:PSS hybrid films is mainly influenced by the addition of GO.

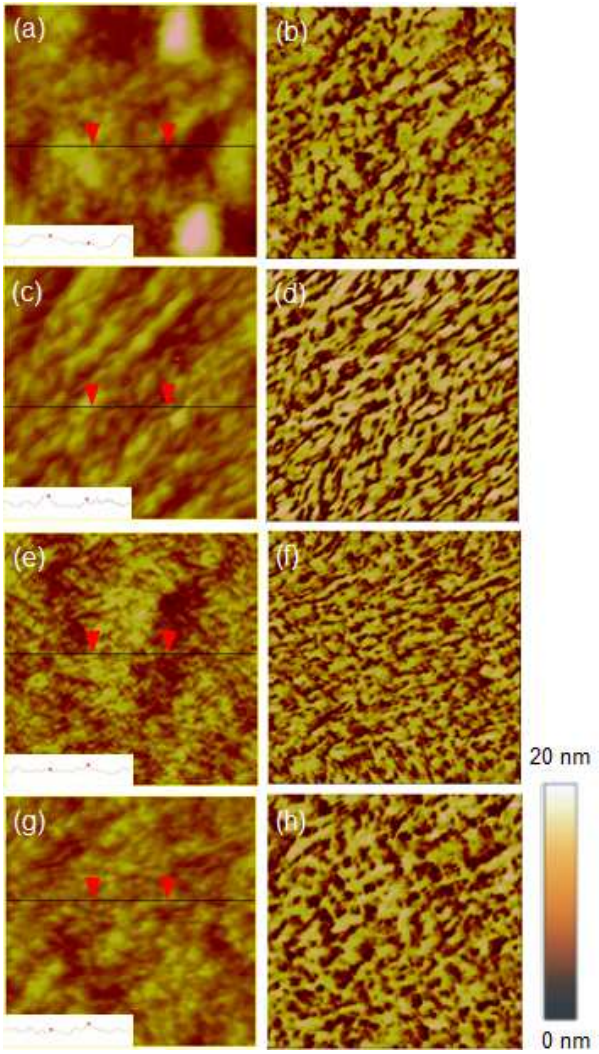

Fig. 5 AFM topographic and phase images of (a-b) PEDOT:PSS with DMSO, the weight ratio of GO:SDBS to PEDOT:PSS is (c-d) 0.01 wt%, (e-f) 0.02 wt%, and (g-h) 0.04 wt%.

In order to further investigate phase separation between PEDOT and PSS, measurements of AFM topographies and phase images were conducted. As shown in Fig. 5, the bright and dark domain, corresponding to PEDOT-rich grains and PSS-rich grains, are observed in phase images.[28] With increasing the ratio of GO:SDBS to 0.02 wt%, the shape of PEDOT-rich grains transforms from short curved domain to long stretched network. 17 It indicates that moderate GO:SDBS can deplete the insulating PSS and generate larger contact areas between oriented PEDOT-rich grains, and this structure can add more conductive pathways for carriers to improve conductivity of the film. However, the shape of PEDOT-rich grains changes to short curved domain again with the addition of GO:SDBS up to 0.04 wt%. Probably the excessive GO nanosheets cause more serious phase separation of PEDOT:PSS and influence the formation of oriented PEDOT-rich grains. Moreover, the roughness of hybrid film reduces with the addition of GO:SDBS. When the addition of GO:SDBS is 0.02 wt%, the roughness of film is only 1.32 nm, which is much lower than that of the pristine PEDOT:PSS film (2.75 nm).

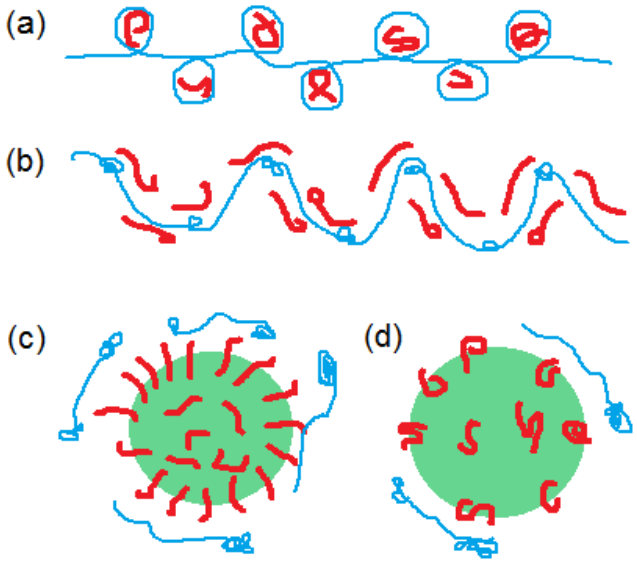

Fig. 6 Conformations of PEDOT:PSS (a) before and after mixing with (b) DMSO and (c) 0.02 wt%, (d) 0.04 wt% GO. The thin blue and thick red curves stand for PSS and PEDOT chains, respectively. The green round sheet stands for GO nanosheet.

The conductivity enhancement of PEDOT:PSS doped with GO:SDBS hybrid films can mainly be attributed to the separation of PSS and PEDOT chains, and separated PEDOT chains can bond with GO nanosheets to extend the conductive network. It is confirmed that in primitive PEDOT:PSS, excess PSS is added in PEDOT:PSS aqueous solution to enable the stable dispersion of hydrophobic PEDOT chains in water. Here PEDOT chains attach to the PSS chain through the coulombic attraction. In order to obtain minimum interactions between PEDOT and water, the PSS segments together with attached PEDOT chains have a coiled conformation as blobs to prevent the contact of PEDOT from water. Meanwhile, the coulombic repulsions among the PSS make the PSS segments without attached PEDOT serve as the strings between blobs (Fig. 6 (a)).[29]

When the DMSO is added into primitive PEDOT:PSS solution, the PEDOT and PSS chains are separated. The PEDOT chains are surrounded dominantly by DMSO, and the PSS chains by water. The coulombic attraction between PEDOT and PSS chains is effectively weakened. Consequently, the coulombic repulsions among the positive (or negative) charges in the PEDOT (or PSS) chain become the dominant factor for the chain conformation, so that both PEDOT and PSS change to the linear and extended-coil conformation (Fig 6 (b)). The linear PEDOT chains have stronger inter-chain interactions, which helps the inter-chain charge transport. However, due to the coulombic repulsions among PEDOT chains the overlap of the PEDOT chains is limited, which affects the formation of more conductive pathways.

There are lots of functional groups (such as –COOH and –OH) on GO nanosheets. These small functional groups can effectively separate PSS and PEDOT chains.[29,30] Consequently, adding the GO into PEDOT:PSS solution can further reduce the coulombic attraction between PEDOT and PSS chains and improve the formation of the linear and extended-coil conformation of PEDOT and PSS chains. Because of the negatively charged carboxyl groups and SDBS on GO sheets, the GO sheets are mainly with negative charge. Therefore, the negatively charged

PSS chains dissolve in water, while positively charged insoluble PEDOT chains will bond with GO nanosheets through coulombic attraction. Moreover, the PEDOT chains mainly change to the linear conformation due to the coulombic repulsions among themselves (Fig 6 (c)). The bonding of GO sheets and linear PEDOT can help to form more conductive pathways. Therefore the conductivity of PEDOT:PSS doped with a small amount of GO:SDBS hybrid film is increased. The structure is in accord with the phase shape shown in AFM phase images, where the shape of PEDOT-rich grains shows long stretched network at the ratio of GO:SDBS to 0.02 wt% (Fig. 5 (f)). However, with the addition of GO:SDBS up to 0.04 wt%, more functional groups on GO nanosheets can bond with PEDOT chains by coulombic attraction. Therefore, the coulombic repulsions among the positive charges in the PEDOT chains are reduced due to less amount of PEDOT chains distributed on each GO nanosheets, and these PEDOT and GO segments together have a coiled conformation as blobs (Fig. 6 (d)). The result is in consistent with the phase shape shown in Fig. 5 (h), where the shape of PEDOT-rich grains shows short curved domain again. These PEDOT blobs and more isolated functional groups on GO nanosheets will reduce the conductive network and lower down the conductivity of the hybrid films.

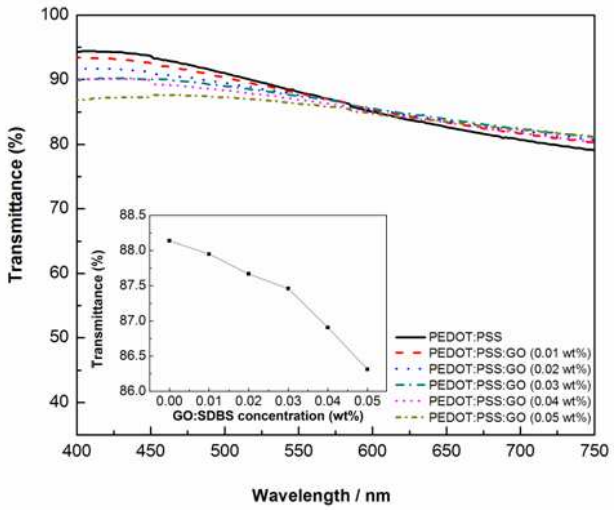

Fig. 7 Transmission spectra and collected transmittance at 550 nm (inset) of PEDOT:PSS films with different doping concentrations of GO:SDBS (0-0.05 wt%).

Fig. 7 shows the transmittance of PEDOT:PSS and GO:SDBS hybrid films. The transmittance measured at 550 nm decreases with the increasing concentration of GO:SDBS. However, the transmittance of hybrid film with highest GO:SDBS concentration (0.05 wt%) is still beyond 86% at 550 nm. The PEDOT:PSS hybrid film doped with 0.02 wt% GO:SDBS can obtain the sheet resistance of 85 ohm per square and transmittance of 87%, which is comparable to ITO.

To show the flexibility characteristic of ITO and PEDOT:PSS hybrid conductive film, bending tests were conducted on PEN substrate. The bending radius is about 8 mm, and one bending cycle includes a concave and a convex compression.[31] The sheet resistance of PEDOT:PSS hybrid films was measured for every 50 times bending cycles. As shown in Fig. 8 (a), the sheet resistance of PEDOT:PSS hybrid films has only 10% increase after 1000 bending cycles, and no cracking is observed from the surface of films, which indicates that the hybrid film is highly flexible and resistant to bending fatigue. On the other hand, as shown in Fig. 8 (b), the sheet resistance of ITO film increases quickly with bending. Due to fragility and inflexibility, the sheet resistance of ITO film increases by 2 orders of magnitude after 10 bending cycles.

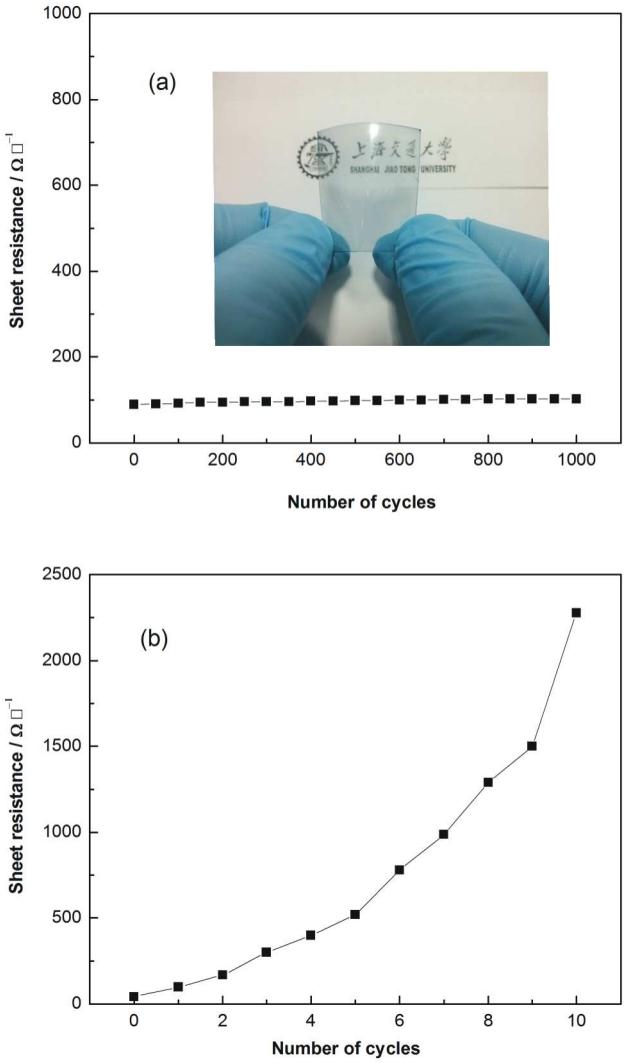

Fig. 8 The bending tests of (a) PEDOT:PSS hybrid film with 0.02 wt% GO:SDBS and (b) ITO on PEN.

Using PEDOT:PSS hybrid films mixed with different ratios (0 wt%, 0.01 wt%, 0.02 wt% and 0.04 wt%) of GO:SDBS as anodes, we fabricated OLED devices with structure illustrated in Fig. 1. The current density-voltage (J-V) curves of OLEDs are shown in Fig. 9 (a). The device with ITO anode has the lowest current density, while those using PEDOT:PSS hybrid anode have much higher current density. The highest one is obtained when 0.02 wt% GO:SDBS is added, which is consistent with the conductivity results. It indicates that the PEDOT:PSS hybrid anodes with high work function (5.1 eV-5.2 eV) facilitate hole injection compared to the ITO anode with low work function (4.4 eV-4.5 eV).[32] On the other hand, the performance of OLED is greatly improved when a hybrid anode with higher conductivity

is employed. A considerably low conductivity limits the current flowing through the OLED device, and results in the reducing of current density.[33] It is found that the leakage current is very small in the exponential curve, which confirms that the fantastic dispersion of GO:SDBS in PEDOT:PSS solution results in the formation of PEDOT:PSS hybrid films with low roughness. As shown in Fig. 9 (b), the device with PEDOT:PSS hybrid anode doped 0.02 wt% GO:SDBS reaches a luminance of 1000 cd m^{-2} only at 4.6 V, and this voltage is much lower than those of other devices. The current efficiencies of the devices show similar trend as the current density characteristics (Fig. 9 (c)), indicating higher current density leads to higher current efficiency. The current efficiency is mainly decided by the charge balance of the whole device, and improving hole injection can obtain better charge balance for this structure. As discussed above, the device with PEDOT:PSS doped with 0.02 wt% GO:SDBS hybrid anode has the best charges transport capability, and the current efficiency reaches 2.7 cd A^{-1} at 100 mA cm^{-2}, which is 70% higher than the best value of the device with ITO anode. Due to lower operating voltage, the power efficiency improvement of the device using PEDOT:PSS hybrid anodes is even higher (Fig. 9 (d)). A maximum power efficiency of 1.8 lm W^{-1} is obtained, which is a factor of 3.6 as high as that of the device with ITO anode (0.5 lm W^{-1}).

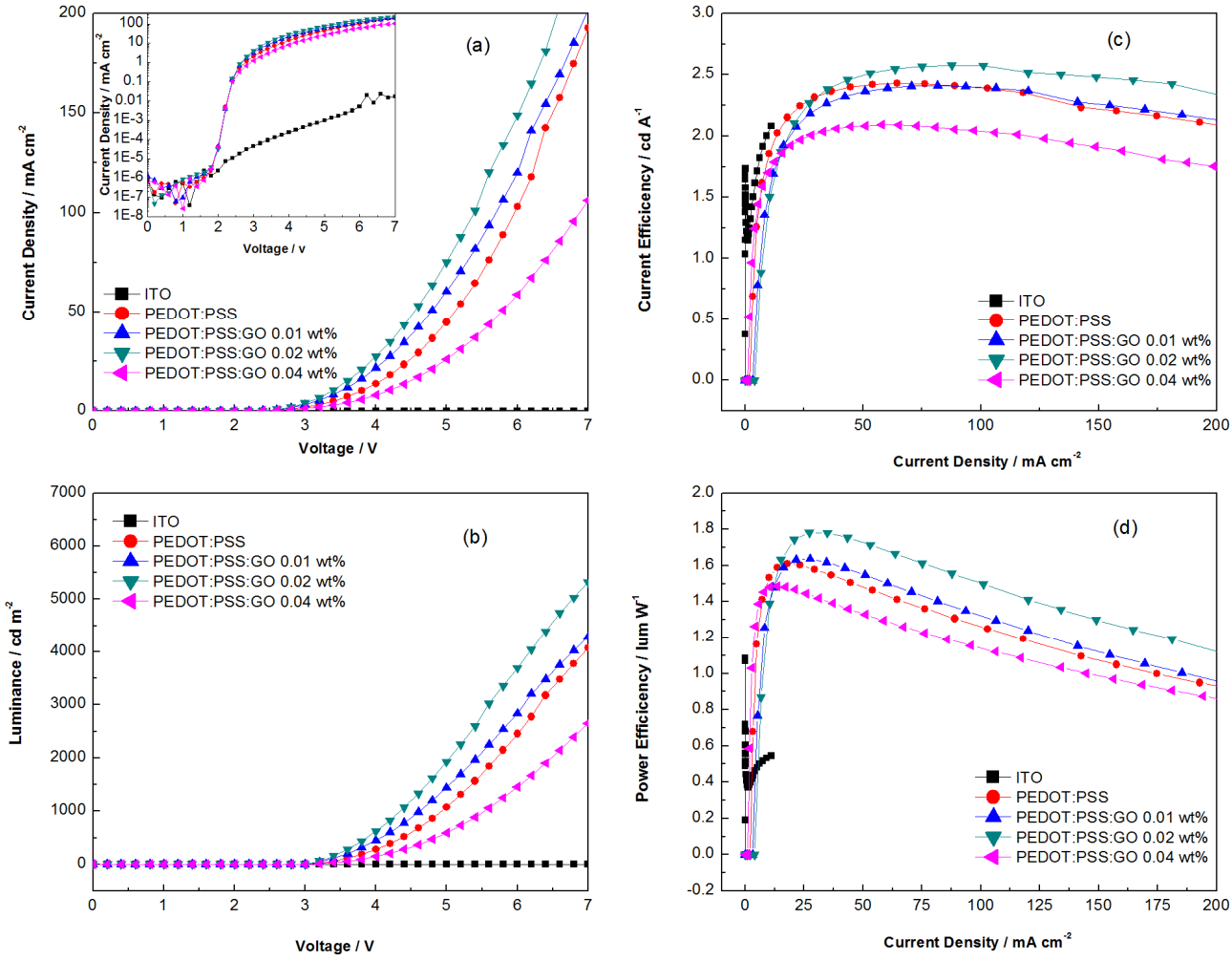

Fig. 9 (a) Current density vs. voltage curves (b) Luminance vs. current density curves (c) Current Efficiency vs. current density curves (d) Power Efficiency vs. current density curves of OLED devices with anodes made by ITO, PEDOT:PSS, and PEDOT:PSS with 0.01 wt%, 0.02 wt% and 0.04 wt% GO:SDBS hybrid films.

4. Conclusion

In conclusion, we successfully improved the conductivity, stability and roughness of PEDOT:PSS hybrid anodes by mixing GO:SDBS solution. PEDOT:PSS hybrid film with 0.02 wt% GO:SDBS has the highest conductivity of 800 S cm^{-1}. The effects are attributed to the shifty phase structures of PEDOT-rich grains and formation of better conductive network by moderate GO nanosheets. Excessive GO:SDBS will interfere with the conductive pathways for carriers. Using these highly conductive and uniform PEDOT:PSS hybrid anodes, OLEDs have been produced on glass and PEN substrates. The variation trend of OLED device performances with PEDOT:PSS hybrid anodes is mainly conformed to the change of conductivity. These results indicate that GO:SDBS and PEDOT:PSS hybrid films with high conductivity, good transmittance and low roughness are highly promising alternative to ITO for low cost and flexible

OLEDs.

5. Acknowledgement

The present work was supported by the National Natural Science Foundation of China (61377030) and the Science and Technology Commission of Shanghai Municipal (12JC1404900). The authors would like to thank Mrs Huiqin Li from the Instrumental Analysis Center of SJTU for helping with the AFM measurements.

Notes and References

[a] *National Engineering Lab for TFT-LCD Materials and Technologies, and Department of Electronic Engineering, Shanghai Jiao Tong University, Shanghai 200240, People's Republic of China. E-mail: gufenghe@sjtu.edu.cn.*

[b] *School of Chemistry and Chemical Engineering, Shanghai Jiao Tong University, 800 Dongchuan Road, Shanghai, 200240, People's Republic of China.*

1. L. W. Peng, Y. Y. Feng and W. Feng, *Journal of Physical Chemistry C*, 2012, **116**, 4970.
2. S. W. Shi, V. Sadhu, R. Moubah, G. Schmerber, Q. Y. Bao and S. Ravi, P. Silva, *Journal of Materials Chemistry C*, 2013, **1**, 1708.
3. B. R. Lee, J. S. Kim, Y. S. Nam, H. J. Jeong and M. H. Song, *Journal of Materials Chemistry C*, 2012, **22**, 21481.
4. C. Merlet, B. Rotenberg, P. A. Madden, P. L. Taberna, P. Simon, Y. Gogotsi and M. Salanne, *Nature Materials,* 2012, **11**, 306.
5. D. Kim, J. Y. Han, D. Lee, Y. Lee and D. Y. Jeon, *Journal of Materials Chemistry* , 2012, **22**, 20026.
6. Y. Wang, S. W. Tong, X. F. Xu, B. Özyilmaz, and K. P. Loh, *Advanced Materials*, 2011, **23**, 1514.
7. D. Q. Zhang, R. R. Wang, M. C. Wen, D. Weng, X. Cui, J. Sun, H. X. Li, and Y. F. Lu, *Journal of Materials Chemistry,* 2012, **134**, 14283.
8. J. V. D. Groep, P. Spinelli, and A. Polman, *Nano Letter*, 2012, **12**, 3138.
9. Johannes, Krantz, T. Stubhan, M. Richter, S. Spallel, I. Litzov, G. J. Matt, E. Spiecker and C. J. Brabec, *Advanced Function Materials*, 2013, **23**, 1711.
10. I. Lahiri, V. P. Verma and W. Choi, *Carbon*, 2011, **49**, 1614.
11. P. H. Wöbkenberg, G. Eda, D. S. Leem and J. C. D. Mello, *Advanced Materials*, 2011, **23**, 1558.
12. B. H. Zhang, G. P. Tan, Z. Y. Xie, W. Y. Wong, J. Q. Ding, and L. X. Wang, *Advanced Materials*, 2012, **24**, 1873.
13. D. Alemu, H. Y. Wei, K. C. Ho and C. W. C, *Energy Environmental Science*, 2012, **5**, 9662.
14. Y. J Xia, H. M. Zhang and J. Y. Ouyang, *Journal of Materials Chemistry*, 2010, **20**, 9740.
15. Y. J. Xia and J. Y. Ouyang, *Macromolecules*, 2009, **42**, 4141.
16. M. Vosgueritchian, D. J. Lipomi, and Z. N. Bao, *Advanced Function Materials*, 2012, **22**, 421.
17. Y. H. Kim, C. Sachse, M. L. Machala, C. May, L. M. Meskamp and K. Leo, *Advanced Function Materials*, 2011, **21**, 1076.
18. W. Gaynor, G. F. Burkhard, M. D. McGehee and P. Peumans, *Advanced Materials*, 2011, **2**, 2905.
19. H. X. Chang, G. F. Wang, A. Yang, X. M. Tao, X. Q. Liu, Y. D. Shen, and Z. J. Zheng, *Advanced Function Materials*, 2010, **20**, 2893.
20. K. Y. Jo, T. Lee, H. J. Choi, J. H. Park, D. J. Lee, D. W. Lee, and B. S. Kim, *Langmuir,* 2011, **27**, 2014.
21. Y. G. Seol, T. Q. Trung, O. J. Yoon, I. Y. Sohn and N. E. Lee, *Journal of Materials Chemistry*, 2012, **22**, 23759.
22. G. H. Zeng, Y. B. Xing, J. Gao, Z. Q. Wang, and X. Zhang, *Langmuir*, 2010, **26**, 15022.
23. P. Matyba, H. Yamaguchi, G. Eda, M. Chhowalla, L. Edman, and N. D. Robinson, *Acs Nano*, 2010, **4**, 637.
24. Y. Wang, S.W. Tong, X. F. Xu, B. Özyilmaz, and K. P. Loh, *Advanced Materials*, 2011, **23**, 1514.
25. S. V. Rodil, J. I. Paredes and A. M. Alonso, *Journal of Materials Chemistry*, 2009, **19**, 3591.
26. B. H. Fan, Y. J. Xia and J. Y. Ouyang, *Proceedings of SPIE*, 2009, 74151.
27. Y. J. Xia, K. Sun and J. Y. Ouyang, *Energy Environmental Science*, 2012, **5**, 5325.
28. A. Benor, S. Y. Takizawa, C. P. Bolívar and P. Anzenbacher, *Organic Electronics*, 2010, **11**, 938.
29. Y. J. Xia and J. Y. Ouyang, *Applied Materials Interface*, 2010, **2**, 474.
30. Y. J. Xia and J. Y. Ouyang, *Journal of Materials Chemistry*, 2011, **21**, 4927.
31. H. J. Lee, T. H. Park, J. H. Choi, E. H. Song, S. J. Shin, H. Kim, K. C. Choi, Y. W. Park and B. K. Ju, *Organic Electronics*, 2013, **14**, 416.
32. C. H. Lin, K. T. Chen, J. R. Ho, J. W. J. Cheng, and R. C. C. Tsiang, *Journal of Nanotechnology*, 2012, **2012**, 942629.
33. W. H. Kim, A. J. Mäkinen, N. Nikolov, R. Shashidhar, H. Kim, and Z. H. Kafafi, *Applied Physics Letters*, 2002, **80**, 3844.

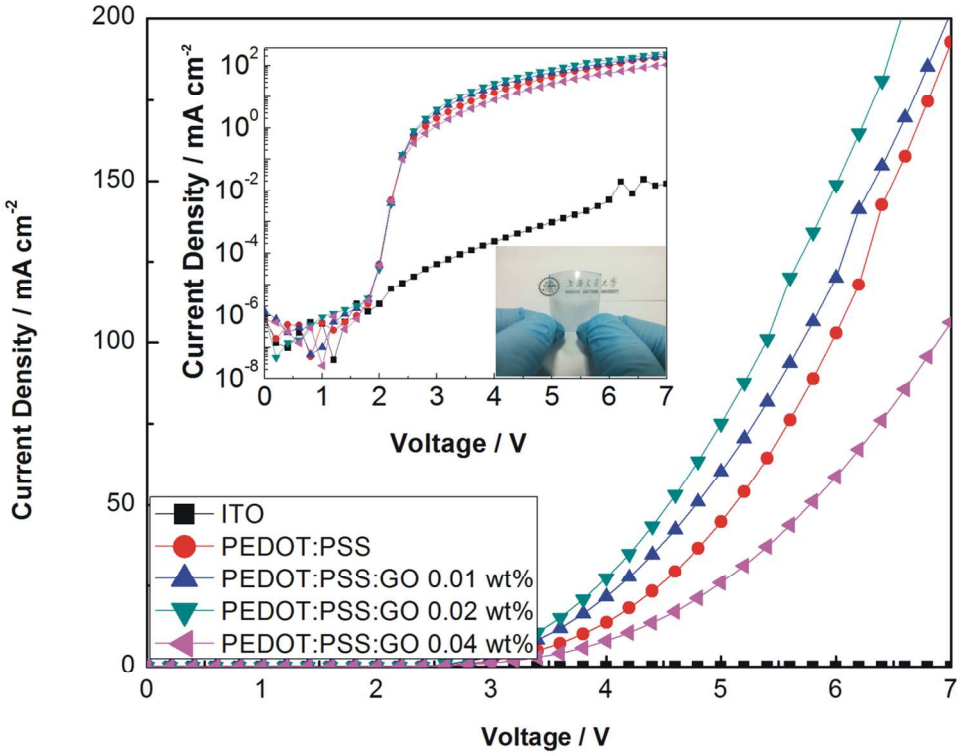

120x92mm (300 x 300 DPI)